Optics Letters

Resonant optical propulsion of a particle inside a hollow-core photonic crystal fiber

A. V. Maslov

University of Nizhny Novgorod, Nizhny Novgorod 603950, Russia (avmaslov@yandex.ru)

Received 12 May 2016; revised 5 June 2016; accepted 5 June 2016; posted 6 June 2016 (Doc. ID 265076); published 28 June 2016

Resonant propulsion of small nonresonant particles inside metal waveguides due to the formation of resonant states by the guided modes below their cutoffs has been predicted in the past. Here it is shown that stable resonant propulsion exists in hollow-core photonic crystal fibers, which are all-dielectric structures and are a major platform for various photonic applications. Specific features of the resonant propulsion are discussed together with the fiber design issues. The results may enable power-efficient transport of particles over long distances, particle sorting, and sensitive detection. © 2016 Optical Society of America

OCIS codes: (140.7010) Laser trapping; (350.4855) Optical tweezers or optical manipulation; (060.5295) Photonic crystal fibers.

http://dx.doi.org/10.1364/OL.41.003062

The optical propulsion of particles inside hollow-core waveguiding structures [see Fig. 1(a)] has emerged as a promising way of their controllable transport over long distances [1–6]. In contrast to focused beams used for particle trapping and propulsion in free space or a liquid environment [7,8], the guided modes do not suffer from the diffractional spreading that puts severe limits on the propulsion range and can also create axial trapping near the waist of the focused beam [9]. Guided modes of fiber capillaries were used for transporting atoms [1], solid particles, and liquid droplets [2]. Compared to open waveguiding structures, such as channeled waveguides [10], strip waveguides [11,12], or optical fiber tapers [13,14], hollow-core fibers offer additional flexibility for laser guidance because the fiber walls control the transport environment by shielding the particles from the surrounding fluid motion [2]. To extend the range of laser-assisted guidance limited in the capillaries by the leakage losses, hollow-core photonic crystal fibers (HC-PCFs) were applied for transporting various particles [3,4], including blood cells [5]. Recently, particles trapped inside HC-PCFs were used as sensors of an external electric field [6].

A rather small refractive index contrast and small size of common particles result in weak scattering, either in free space or inside waveguides, and therefore, weak optical forces as compared to the momentum flow of the incident light. Scattering can be increased substantially when the particles possess resonances, such as plasmon resonances in metal particles, Mie resonances in high-index dielectric particles, or whispering gallery mode (WGM) resonances in large dielectric particles. However, the requirement of having resonances significantly limits the variety of particles that can be efficiently propelled.

Guiding structures offer another mechanism for enhancing the optical forces on particles without intrinsic resonances. The particles can give strong scattering in the regimes where they form resonant states with the guided modes below their cutoffs. The resonant scattering from inhomogeneities inside metal waveguides is used in narrow-band microwave filters [15]. According to the conservation of the electromagnetic momentum, the resonant reflection should result in a large force on the inhomogeneity. The force on a pointlike scatterer (cylinder) [16] and on small high-index dielectric cylinder [17] inside a parallel-plate waveguide for the transverse electric (TE) polarization in the two-dimensional (2D) geometry were investigated. The optical forces on particles of arbitrary sizes were studied in Refs. [18–20]. The appearance of resonant reflection from waveguide inhomogeneities, such as particles, is analogous to resonant reflection from periodic gratings (Wood's anomalies) where the resonant excitation of leaky modes takes place [21]. A fourfold enhancement of the propulsion velocities was also realized by changing the wavelength in slow light photonic crystal waveguides without resonant features [22].

So far, the hybrid particle-waveguide resonances have been explored only for the cases of parallel-plate [16,19,20] or cylindrical waveguides [20] with metal walls. Although the resonant enhancement of particle propulsion in metal waveguides seems possible, all-dielectric structures, such as HC-PCFs, are more common in practice [3–6]. However, the dispersion characteristics of HC-PCFs and metal waveguides differ significantly. The guiding properties of HC-PCFs are provided by reflection from the periodic walls that give total reflection only in limited ranges of frequencies and angles. A natural question arises: whether any resonant enhancement of particle propulsion is

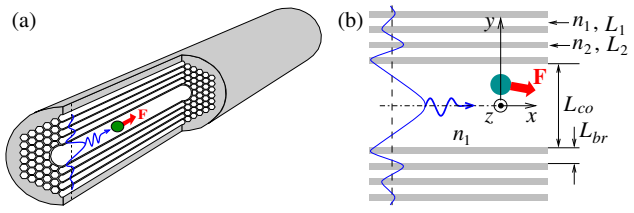

Fig. 1. (a) Schematic view of particle propulsion inside a HC-PCF. (b) 2D propulsion model and parameters.

possible in HC-PCFs. The existence of resonant propulsion has not been established in such situations, and this problem is addressed in this Letter.

It is shown here that the resonant and stable propulsion in HC-PCFs is possible, and specific conditions to realize it are discussed. The study is based on a 2D model. The model reproduces well basic properties of HC-PCFs and accounts fully for the particle interaction with the walls. Such interaction is often neglected in estimating the propelling and trapping forces due to the difficulty to account for it; the scattering is calculated using ray optics with the intensity distribution determined by the guided mode [2–4]. When the particle size, core diameter, and wavelength are comparable, a common situation for particles inside HC-PCFs, this interaction is important and, in fact, is the basis for the resonant properties described here.

The 2D model for the particle propulsion inside a HC-PCF is shown in Fig. 1(b). The HC-PCF is represented by two periodic structures (Bragg reflectors) separated by a core region. The Bragg reflectors (BRs) are formed by an infinite number of layers with refractive indices $n_{1,2}$ and thicknesses $L_{1,2}$ so that $L_{\rm br} = L_1 + L_2$ is the period. The core region has index n_1 and width $L_{\rm co}$. Since the properties of plane BRs are similar to those in microstructured fibers, the 2D model is often used to study various optical characteristics of HC-PCFs, including light coupling between photonic crystal fibers and photonic bandgap circuits [23]. The particle has index n_p, radius R, and is located at y_0. We consider the case when the electric field is polarized along the z axis (TE polarization). An incident-guided mode is scattered by the particle. This creates an optical force that has longitudinal (propelling) and transverse (trapping) components. We take $n_1 = 1$, $n_2 = n_p = 1.5$ in all cases.

To find the force, we solve the scattering problem analytically using the approach applied in Refs. [19,20] for modeling metal waveguides. The polarization induced inside the particle is expanded into cylindrical functions. The field emitted by the polarization is reflected from the walls at $y = \pm L_{\rm co}/2$ and is incident back on the particle. The correspondence between the created total field and the assumed polarization gives a system of linear equations from which the expansion coefficients can be calculated numerically. It is a quite general analytical approach, and its results agree well with finite-difference time-domain simulations [19]. Similar approaches are used for analytical treatment of guided-mode scattering on various inhomogeneities [24–27]. Compared to the case of metal walls, one needs to replace the reflection coefficient $r = -1$ from metal with the much more complicated Bragg reflection coefficient that depends both on frequency and in-plane wavenumber (or angle) of the incident wave. The coefficient is calculated from the impedance of the Bloch modes obtained using the transfer matrix approach. The reflection coefficient has to be calculated not only for propagating waves (with real incident angles), but also for evanescent waves (with imaginary incident angles) in the core region. After the scattering problem is solved, the optical forces can be calculated using the momentum balance, Lorentz formula, or Maxwell tensor.

The dispersion properties of the guided modes can be obtained using the reflection phase φ_r in the regions of BR total reflection from the phase condition $\varphi_r + kL_{\rm co}\sqrt{n_1^2 - n_{\rm ph}^2} = m\pi$, where $m = 1, 2, 3\ldots$, $k = \omega/c$, and $n_{\rm ph}$ is the phase (or effective) index for the guided modes The dispersion curves for several lowest order symmetric and antisymmetric (with respect to E_z) modes for $L_{\rm br}/L_{\rm co} = 0.25, 0.39$ are shown in Fig. 2. The number of modes increases with $L_{\rm co}/\lambda$. Unlike the case of metal waveguides, the dispersion curves exist only in the limited ranges of parameters that correspond to the bandgaps of the BRs. The curves can start either from $n_{\rm ph} = 0$ or near the edges of the bandgap regions. The bandgap regions are curved, and one can easily evaluate the propagation angles where the BRs are only partially reflective. There are large areas in the dispersion diagram where no guided modes exist. In the case of metal waveguides, each subsequent mode of a fixed symmetry adds one period of field oscillation. This rule does not work in the case of BRs. The lowest mode in both cases shown in Fig. 2 is symmetric, and its phase index is close to 1.

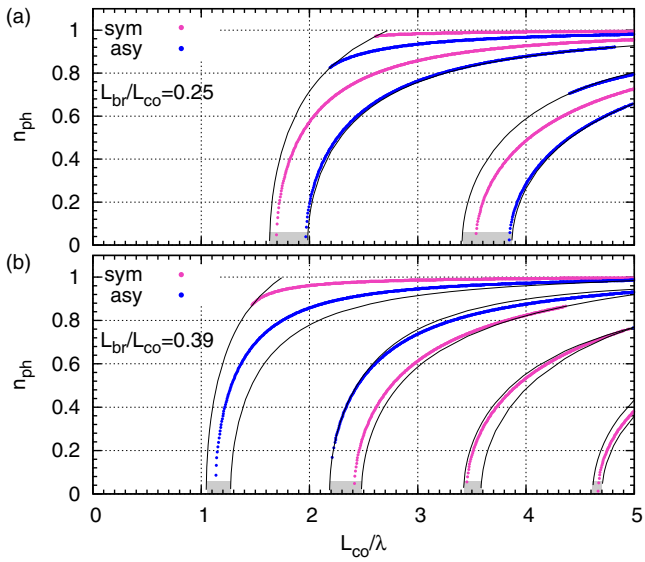

Fig. 2. Dispersion for the symmetric (sym) and antisymmetric (asy) guided modes for (a) $L_{\rm br}/L_{\rm co} = 0.25$ and (b) $L_{\rm br}/L_{\rm co} = 0.39$. The black lines show the band edges and shaded areas show the bandgaps at $n_{\rm ph} = 0$. The BR parameters are $L_1/L_{\rm br} = 0.8$, $n_1 = 1$, $n_2 = 1.5$.

To understand the peculiarities of scattering and forces for HC-PCFs, let us look at the main features of the resonant propulsion of a particle inside a metal waveguide (see Fig. 3). To evaluate the propulsion efficiency, the force is normalized to P_0/c, where P_0 is the incident power. A resonant peak is formed just below the cutoff for the second symmetric mode at $L/\lambda = 3/2$. The peak reaches the value of about $cF_x/P_0 = 1.88$. The phase index of the modes is

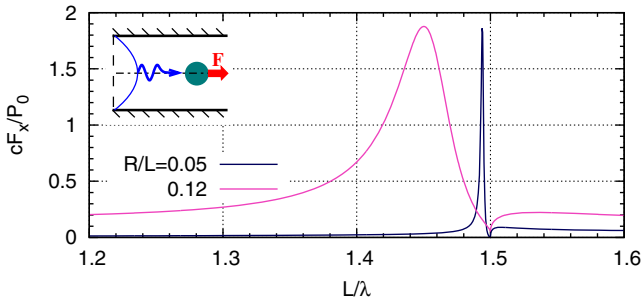

Fig. 3. Propelling force cF_x/P_0 on a particle in the center of a metal waveguide with width L as a function of L/λ.

$n_{ph} = \sqrt{1 - (m\lambda/(2L))^2}$, where $m = 1, 2, 3\ldots$. For the incident fundamental TE mode with $m = 1$ at $L/\lambda = 1.45$, the index is $n_{ph} = 0.94$. Thus, the maximum of F_x agrees well with twice the value of the momentum flow $n_{ph}P_0/c$. The incident mode is totally reflected at resonance. As the particle becomes smaller, the peak becomes narrower and moves closer to the cutoff.

Moving now to the scattering inside a HC-PCF, we assume that its lowest mode is incident on a particle in the center, $y_0 = 0$. The scattering results in the formation of reflected and transmitted signals in the same mode as the incident one, other guided modes propagating in both directions, and waves that are transmitted through the BRs. The total guided power in the forward direction (transmitted in the lowest mode P_t and scattered P_{sf} into all other propagating guided modes) and propelling force for $L_{br}/L_{co} = 0.25, 0.39$ are shown in Figs. 4 and 5. Because of $y_0 = 0$, only the symmetric modes can be excited.

Looking at the case $L_{br}/L_{co} = 0.25$, Fig. 4, one can clearly see a strong reduction in the forward power just below the cutoff frequency ($L_{co}/\lambda = 3.535$) for the third symmetric mode [see also Fig. 2(a)]. At $L_{br}/L_{co} = 0.25$, $L_{co}/\lambda = 3.52$, the phase index of the incident mode is $n_{ph} = 0.989$, and the ratio of the power in the core region and the total power is $P_{co}/P_0 = 0.99$. The maximum reduction of the transmitted power is significant, reaching almost 40%, but not complete, as in the case of metal waveguides [19,20]. The dips are highly asymmetric. The decrease in the forward power corresponds to the enhancement of the propelling force. For the small particles, $R/L_{co} = 0.03$ and $R/L_{co} = 0.05$, the propelling force reaches $cF_x/P_0 \approx 0.52$. As the size decreases, the peak becomes very narrow and moves very close to the cutoff of the third mode. For the larger particles, $R/L_{co} = 0.1$ and $R/L_{co} = 0.12$, the resonant features of propulsion slowly disappear.

The scattering and propulsion for $L_{br}/L_{co} = 0.39$ are shown in Fig. 5. While the general spectral features in both cases, $L_{br}/L_{co} = 0.25, 0.39$, are similar, the latter case clearly shows much stronger resonant features. At $L_{br}/L_{co} = 0.39$,

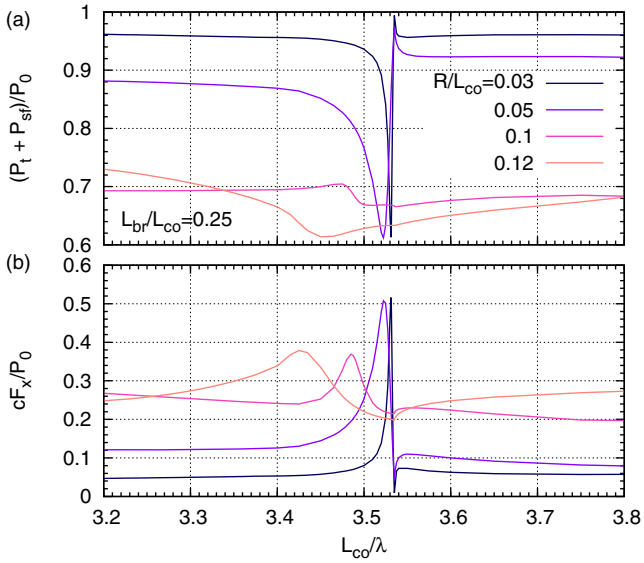

Fig. 4. Scattering on a particle in the center of a HC-PCF with $L_{br}/L_{co} = 0.25$ for several values of R/L_{co}. (a) Forward-guided power as a function of L_{co}/λ. (b) Propelling force on the particle. The key in frame (a) refers to both frames.

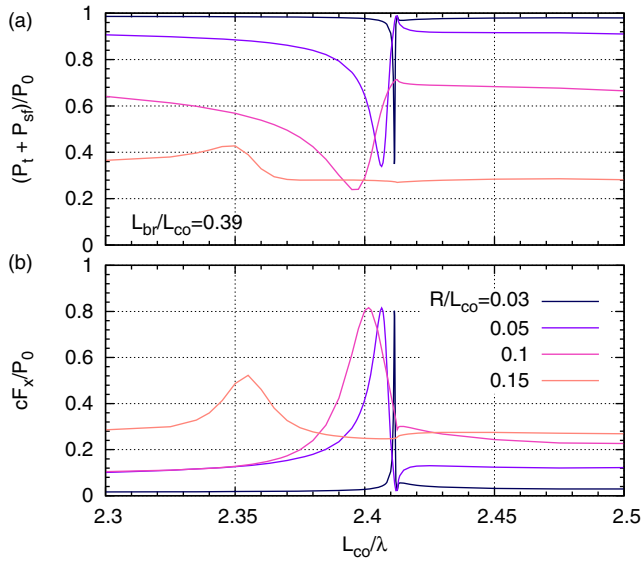

Fig. 5. Same as Fig. 4 but for $L_{br}/L_{co} = 0.39$.

$L_{co}/\lambda = 2.41$, the phase index of the incident mode is $n_{ph} = 0.976$, and the ratio of the power in the core region and the total power is $P_{co}/P_0 = 0.971$. The resonant force can reach values $cF_x/P_0 \approx 0.8$. While this maximum value is still below the ultimate limit $cF_x/P_0 = 2$ or slightly smaller value $cF_x/P_0 = 1.88$ in Fig. 3, the resonant enhancement remains very significant. For example, at $R/L_{co} = 0.05$, the maximum force is about 8 times larger than its value away from resonance at $L_{co}/\lambda = 2.3$. Even much larger resonant enhancement is observed for $R/L_{co} = 0.03$ but the peak is extremely narrow.

The stronger resonance at $L_{br}/L_{co} = 0.39$ compared to that at $L_{br}/L_{co} = 0.25$ can be attributed to the dispersion properties of the fibers (see Fig. 2). Indeed, at $L_{br}/L_{co} = 0.39$, the cutoff frequency, below which the resonance takes place, lies deeper in the bandgap of the BRs. As a result, the angular range of waves experiencing total reflection is larger, making the case closer to that of metal waveguides.

The appearance of large propelling forces on a particle is only one requirement to obtain its efficient propulsion. The particle should also be trapped in the transverse direction. Figure 6 shows both the propelling and trapping forces near resonance ($L_{br}/L_{co} = 0.39$, $R/L_{co} = 0.05$, $L_{co}/\lambda = 2.4065$) as functions of the particle displacement in the transverse direction. The transverse force increases linearly as the particle moves from the center and is directed in such a way that it pushes the particle back to the center. Thus, the transverse force traps the particle in the center. At the same time, the propelling force remains at its maximum value. Interestingly, there is another location of the particle, $y_0/L_{co} = 0.21$, where significant and stable propulsion can be realized, but with a reduced efficiency, $cF_x/P_0 = 0.5$.

In order to clarify the origin of various propulsion regimes shown in Fig. 6, the electric field distributions for the relevant modes were calculated (see Fig. 7). The lowest mode, which is incident on the particle, has a maximum in the center. The next symmetric mode just above its cutoff has five intensity maxima: $y/L_{co} = 0, \pm 0.21, \pm 0.41$. Note that the symmetric mode with three maxima, which would exist in the case of metal waveguides, does not exist here due to only partial reflectivity of

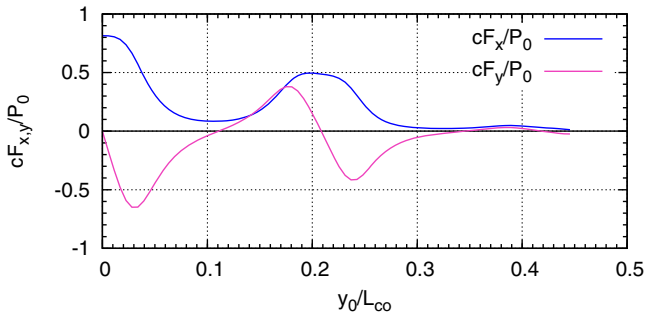

Fig. 6. Propelling and trapping forces as functions of the particle position for $R/L_{co} = 0.05$, $L_{co}/\lambda = 2.4065$, and $L_{br}/L_{co} = 0.39$.

the BRs in the corresponding frequency range. The small particle forms resonant states when it is either at $y_0 = 0$ or at $y_0/L_{co} = \pm 0.21$. The location $y_0/L_{co} = \pm 0.41$ is apparently too close to the BR and no resonant state is formed.

To conclude, it has been shown that a small dielectric particle inside a HC-PCF can be resonantly and stably propelled by a guided mode. The investigation has been carried out within a 2D model, which reproduces the formation of frequency and angle-dependent bandgaps that enable waveguiding in HC-PCFs and accounts self-consistently for the electromagnetic interaction between the particle and BRs. The resonant propulsion can take place just below the cutoff frequencies for the higher order modes, similar to that in parallel-plate [16,19,20] or tube metal waveguides [20]. The resonant propulsion inside HC-PCFs is less efficient due to partial transmission of BRs at some angles of plane wave incidence. The efficiency increases when the cutoff moves away from the BR band edge. The cutoff position away from the BR band edge, which enables the observation of the resonant effects, can be achieved by a judicious design of HC-PCFs. The efficiency of propulsion reaches $cF_x/P_0 \sim 0.5$–0.8 for particles significantly smaller than the core width, $R/L_{co} \lesssim 0.1$. The use of larger particles flattens the resonant features. Although the results were obtained using the 2D model, the predictions are expected to hold in 3D geometry of HC-PCFs, since the model captures correctly all relevant effects. In particular, the predictions of the resonant propulsion for parallel-plate metal waveguides in 2D was shown to hold in 3D cylindrical metal waveguides as well [20].

The resonant propulsion of particles inside all-dielectric waveguiding structures can extend the functionalities of various platforms for chemical and biological analysis [5,28], including particle sorting [12,14,29,30]. Apart from propulsion, the strong resonances in HC-PCFs can also be used to design or monitor the transmission properties of fiber-based systems with particles trapped by guided beams [6] or transverse beams [31]. The formation of resonant features does not require the presence of intrinsic resonances, such as WGM resonances in particles inside microstructured fibers [32], or the modification of the fiber itself as, for example, in the surface nanoscale axial photonics (SNAP) platform [33], and offers new opportunities for optomechanical tuning of photonic devices.

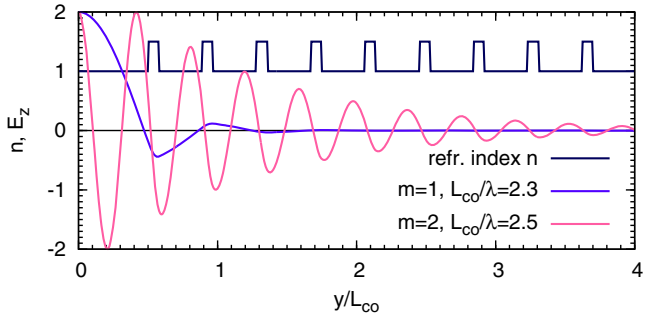

Fig. 7. Refractive index profile for the HC-PCF with $L_{br}/L_{co} = 0.39$ and distributions of $E_z(y)$ for the first (at $L_{co}/\lambda = 2.3$) and second (at $L_{co}/\lambda = 2.5$) symmetric modes.

Funding. Ministry of Education and Science of the Russian Federation (02.B.49.21.0003).

REFERENCES

1. M. J. Renn, D. Montgomery, O. Vdovin, D. Z. Anderson, C. E. Wieman, and E. A. Cornell, Phys. Rev. Lett. **75**, 3253 (1995).
2. M. J. Renn, R. Pastel, and H. J. Lewandowski, Phys. Rev. Lett. **82**, 1574 (1999).
3. F. Benabid, J. C. Knight, and P. St.J. Russell, Opt. Express **10**, 1195 (2002).
4. T. G. Euser, M. K. Garbos, J. S. Y. Chen, and P. St.J. Russell, Opt. Lett. **34**, 3674 (2009); Erratum, *Opt. Lett.* 35, 34 (2010).
5. S. Unterkofler, M. K. Garbos, T. G. Euser, and P. St.J. Russell, J. Biophoton. **6**, 743 (2013).
6. D. S. Bykov, O. A. Schmidt, T. G. Euser, and P. St.J. Russell, Nat. Photonics **9**, 461 (2015).
7. A. Ashkin, Phys. Rev. Lett. **24**, 156 (1970).
8. T. N. Buican, M. J. Smyth, H. A. Crissman, G. C. Salzman, C. C. Stewart, and J. C. Martin, Appl. Opt. **26**, 5311 (1987).
9. A. Ashkin and J. M. Dziedzic, Appl. Phys. Lett. **24**, 586 (1974).
10. S. Kawata and T. Tani, Opt. Lett. **21**, 1768 (1996).
11. S. Gaugiran, S. Gétin, J. M. Fedeli, G. Colas, A. Fuchs, F. Chatelain, and J. Dérouard, Opt. Express **13**, 6956 (2005).
12. B. S. Schmidt, A. H. J. Yang, D. Erickson, and M. Lipson, Opt. Express **15**, 14322 (2007).
13. G. Brambilla, G. Senthil Murugan, J. S. Wilkinson, and D. J. Richardson, Opt. Lett. **32**, 3041 (2007).
14. Y. Li, A. V. Maslov, N. I. Limberopoulos, A. M. Urbas, and V. N. Astratov, Laser Photon. Rev. **9**, 263 (2015).
15. J. N. Sahalos and W. Vafiadis, IEEE Trans. Microwave Theor. Tech. **33**, 1165 (1985).
16. R. Gómez-Medina, P. San José, A. García-Martín, M. Lester, M. Nieto-Vesperinas, and J. J. Sáenz, Phys. Rev. Lett. **86**, 4275 (2001).
17. Z. Wang and P. T. Rakich, Opt. Express **19**, 22322 (2011).
18. A. V. Maslov and M. I. Bakunov, Opt. Lett. **39**, 2823 (2014).
19. A. V. Maslov, Phys. Rev A **92**, 033814 (2015).
20. A. V. Maslov and M. I. Bakunov, Opt. Lett. **40**, 1806 (2015).
21. A. Hessel and A. A. Oliner, Appl. Opt. **4**, 1275 (1965).
22. M. G. Scullion, Y. Arita, T. F. Krauss, and K. Dholakia, Optica **2**, 816 (2015).
23. J. Bauer and S. John, Phys. Rev. A. **77**, 013819 (2008).
24. N. K. Uzunoglu and J. G. Fikioris, J. Opt. Soc. Am. **72**, 628 (1982).
25. A. G. Yarovoy, Microwave Opt. Technol. Lett. **7**, 178 (1994).
26. S. V. Boriskina and A. I. Nosich, Microwave Opt. Technol. Lett. **13**, 169 (1996).
27. V. I. Kalinichev and P. N. Vadov, Radiotekh. Elektron. **33**, 464 (1988).
28. B. S. Ahluwalia, P. McCourt, T. Huser, and O. G. Hellesø, Opt. Express **18**, 21053 (2010).
29. Y. Zhang and B. Li, Laser Photon. Rev. **7**, 289 (2013).
30. A. V. Maslov and V. N. Astratov, Appl. Phys. Lett. **105**, 121113 (2014).
31. P. Domachuk, N. Wolchover, M. Cronin-Golomb, and F. G. Omenetto, Appl. Phys. Lett. **94**, 141101 (2009).
32. K. Kosma, G. Zito, K. Schuster, and S. Pissadakis, Opt. Lett. **38**, 1301 (2013).
33. M. Sumetsky and Y. Dulashko, Opt. Express **20**, 27896 (2012).